Integrating Battery into MMC Submodule Using Passive Technique

Sigurd Byrkjedal Wersland, Anirudh Budnar Acharya, *Member, IEEE* and Lars Einar Norum, *Member, IEEE*

Department of Electrical Power Engineering, Norwegian University of Science and Technology (NTNU)
7491-Trondheim, Norway

***Abstract*—The modular structure and the many other advantages of the Modular Multilevel Converter makes it an attractive converter for Battery Energy Storage Systems, allowing the battery units to be distributed throughout the convert, connected in each submodule. However, such an arrangement results in large oscillating components in the battery current, which is harmful to battery performance and lifetime. In most literature this is solved using DC-DC converters as active interfaces between battery and submodule.**

This paper investigates a passive filter arrangement as an alternative solution to the DC-DC converters. Where the batteries are interfaced with the submodules using a passive filter that suppresses the fundamental component and control technique that injects circulating current to suppress second harmonic component. It is concluded that this passive technique could be an attractive solution especially where high reliability is of concern.

Keywords—Modular Multilevel Converter (MMC); Battery Energy Storage System (BESS); integrated split-battery; circulating current injection; passive filter interface

I. Introduction

Battery Energy Storage System (BESS) provide multiple support to grid applications and are main source of power in other applications such as all electric ships, electric vehicles etc. [1]. In a classical arrangement, the batteries are connected in series and then paralleled to form the low voltage DC source with required power rating. These units are connected to the DC link of 2 or 3 level power converters, where AC side voltage is limited by the low DC voltage.

The Modular Multilevel Converter (MMC) allows battery units to be connected directly into the submodule. Integrating the battery units in a distributed manner throughout the converter (Fig. 1). This arrangement takes advantage of both the modularity of battery units and the converter modular arrangement. This gives one important advantage; The maximum achievable AC side peak voltage is now related to the number N submodules in each arm of the MMC times the battery voltage. Allowing high AC side voltage and at the same time low DC battery voltage.

This is advantageous because battery cells needs to be series connected to reach high voltage. And series connected cells (especially for Li-ion) require Battery Management Systems (BMS) to monitor and balance State Of Charge (SOC) on each level in the series connection, if they are to be operated safely. This increases complexity of the BMS for each added level, finally leading to a maximum achievable battery voltage.

Taking into account that the MMC also features high voltage capabilities, high efficiency and low harmonic distortion finally makes this converter structure attractive to be used also in BESS applications.

The impediment of the split-battery arrangement described in the last section is that the current flowing in the MMC submodules has large oscillating components at low frequency that can be harmful to the battery performance and lifetime. To solve this, the battery can be connected to the submodule using an active interface (DC-DC converter), which can mitigate theses components and provide a fixed DC output, allowing safe battery connection. This method needs an additional DC-DC converter and sophisticated control tuned properly with the MMC control loops [2]. Additionally, if a DC load is present, a separate DC-DC converter is necessary. The active interface, therefore, increases the complexity and decreases the reliability of the converter.

Therefore, in applications requiring high reliability, the passive interface appears to be suitable, at least in the case of the cascaded H-bridge proposed in [3]. This arrangement decreases the number of active components and increases the overall reliability. However, in case of the MMC, as apposed to the CHB, there are two separate low order frequencies present in the submodules. Therefore, this paper presents an alternative solution of injecting a circulating current in the MMC that removes one of the oscillating components and then employ a resonant filter as battery interface, tuned to mitigate the other frequency. Together with a lowpass branch in the filter, this can considerably lower the oscillating components in the battery current.

Another important topic that needs to be considered when realizing an MMC based BESS with integrated split-battery, is battery unit balancing. All the units connected to each submodule requires its own local BMS to balance all the cells. But for the system as a whole, it is also important that all the battery units can be balanced. This requires a higher level of BMS, which needs to be implemented through the control system of the MMC. Balancing across the phases (legs), upper and lower arm, and among submodules can be realized through power control. This is done by controlling the common-mode-

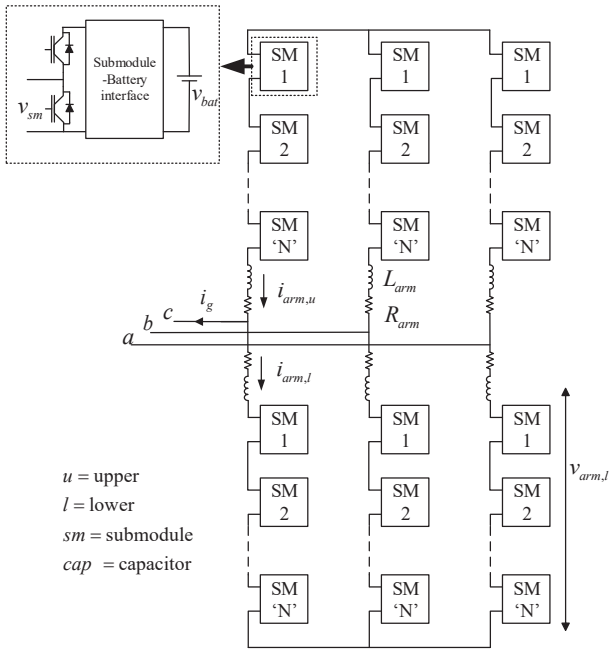

Fig. 1. Modular Multilevel Converter with batteries connected to submodules using passive interfaces

voltage, injecting circulating current at fundamental frequency and index modulation respectively. All these controllers are employed in a regular MMC to ensure balanced submodule capacitors and are adapted to the case of battery balancing in [2] and [4].

These techniques can also be employed when using passive interfaces. But the fact that the passive interface also can be defined as a direct interface, meaning that the battery voltage will have a direct relation to the submodule voltage, results in some additional challenges. **1.** In the case of unbalanced battery units, the MMC needs to be able to operate with different submodule voltages. And **2.** the different currents flowing through the batteries when balancing will also result in differing battery and submodule voltage due to the battery internal resistance.

This finally leads to the necessity of an additional control layer that can counteract the differing submodule voltages, which is necessary to prevent interruption of battery unit balancing and injection of DC current to AC side. This is done in [5] by injecting DC component in the arm voltage references.

This paper is organized as follows. Section I has introduced the proposed passive technique and the split-battery arrangement in an MMC based BESS and identified some issues and advantages. Section II analyses the proposed technique in detail, covering the circulating current injection technique, filter design and some simple loss estimations. Section III presents simulation results and simple lab experiment. Section IV finally concludes the paper.

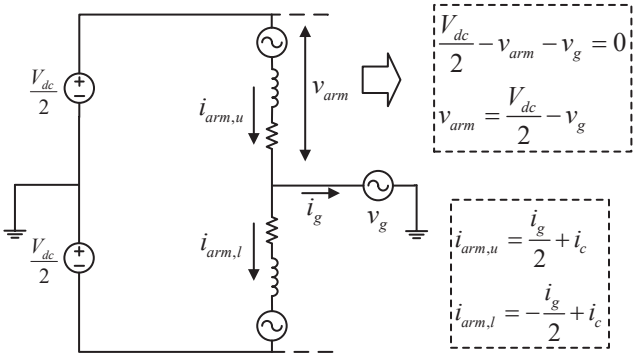

Fig. 2. Simplified MMC circuit, deriving v_{arm} and upper and lower arm currents

II. The passive technique

A. Submodule Current Analysis

To see the power that the submodules need to buffer during operation, which is proportional to the current that would flow through the batteries, lets consider the arm power equation. Using the definitions derived in Fig. 2:

$$P_{arm} = v_{arm} i_{arm} = \left(\frac{V_{dc}}{2} \mp v_g\right)\left(\pm \frac{i_g}{2} + i_c\right) \tag{1}$$

Where i_c is defined as the circulating current that only flows within the legs of a 3-phase MMC. This further developes to:

$$P_{arm} = \frac{V_{dc}}{2}\frac{i_g}{2} + \frac{V_{dc}}{2} i_c - v_g \frac{i_g}{2} - v_g i_c \tag{2}$$

Power in upper arm of Fig. 2 is expressed as (2), but as expressed in (1), first and last term would have opposite signs for lower arm. The last term can potentially produce a DC component if circulating current of fundamental frequency is injected. The circulating current, therefore, enables control of arm power difference. But for this analysis these signs do not make a difference and the characteristics that is to be derived from (2) will represent all the arms.

Circulating current suppression can be achived using several well known techniques [6]. So it is safe to simplify (2) assuming $i_c = 0$.

$$P_{arm} = \frac{V_{dc}}{2}\frac{i_g}{2} - v_g \frac{i_g}{2} \tag{3}$$

Further, using trigonometric identity of product of cosine, (3) can be rewritten as (4) if a modulation index and power factor of unity is assumed, resulting in $\frac{V_{dc}}{2} = \hat{v}_g$ and $\varphi = 0$.

$$P_{arm} = \frac{1}{4}\hat{i}_g \frac{V_{dc}}{2}\left[2\cos(\omega t) - \cos 2\omega t + 1\right] \tag{4}$$

Equation (4) finally show that there are two low frequency components, fundamental and 2nd harmonic, present in the arm power. Having twice and the same peak amplitude in relation to the DC component respectively. Illustrated in Fig. 3, with 50 Hz defined as fundamental frequency.

Current consisting of approximately the same components would flow through the batteries if they where connected

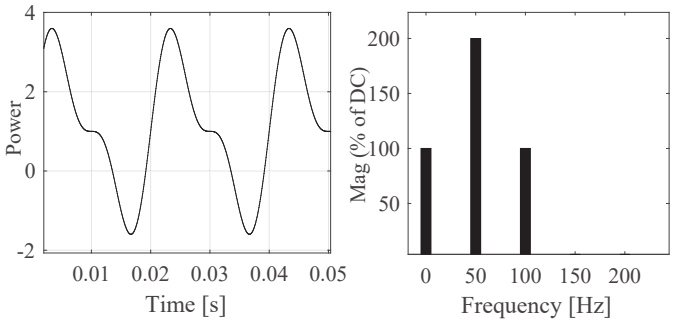

Fig. 3. Illustrated waveform and its FFT from (4)

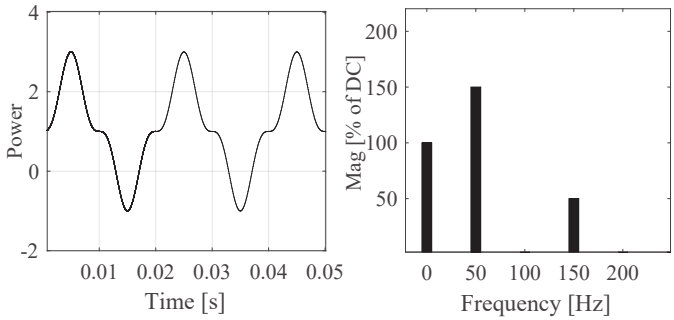

Fig. 4. Illustrated waveform and its FFT from (8)

directly to the submodules. Where only the DC component would do any active power transfer.

Notice also that in regular MMC operation, where power is flowing between the main DC link and the AC side, i_c would contain a DC component. This component cancels the DC component found in (4). In case of the split-battery arrangement considered in this paper, there is no power (current) flowing from the main DC link. Hence resulting in zero DC component in i_c, but a DC component in the arm power instead. Since the power source i.e. the batteries, are place within the arms.

B. Second Harmonic Suppression using Circulating Current

One impediment of the MMC is that the capacitor energy storage requirement is inversely proportional to the output frequency. This is a problem when adapting MMCs to low frequency applications. Therefore in [7] a technique to decouple the arm energy fluctuations from the output frequency for adaption of the MMC to variable speed drives is proposed. Later in [8] a similar technique to reduce peak to peak arm energy fluctuations in the MMC for use in frequency converters in rail power supply is proposed. This technique cancels the second harmonic arm power fluctuation and is also described in [9] and [10].

Therfore, the second harmonic component shown in (4) and Fig. 2 can be mitigated using the technique in [8]. To understand this technique, look at the third term in (2), $v_g\frac{i_g}{2}$, which produces a second harmonic component and a DC component. Since the circulating current only flows within the three converter legs and can be controlled without interfering with AC or DC side, the second term in (2), $\frac{V_{dc}}{2}i_c$, provides the possibility of canceling that second harmonic component by injecting the following circulating current.

$$-v_g\frac{i_g}{2}+\frac{V_{dc}}{2}i_c=0 \tag{5}$$

Only taking into account the oscillating component leads to

$$\begin{aligned} i_c=\frac{v_g i_g}{2\frac{V_{dc}}{2}}&=\frac{\hat{v}_g\hat{i}_g}{V_{dc}}\frac{1}{(\sqrt{2})^2}\Big[\cos(2\omega t+\varphi)+\cancel{\cos(\varphi)}\Big]\\ &=\frac{\hat{v}_g\hat{i}_g}{V_{dc}}\frac{1}{2}\cos(2\omega t+\varphi) \end{aligned} \tag{6}$$

(6) suggests that a circulating current with second harmonic frequency and in phase with the output current will cancel the second harmonic arm power fluctuation.

Injecting this circulating current into (2), assuming $\varphi=0$, will result in the following arm power.

$$\begin{aligned} P_{arm}=&\frac{1}{2}\frac{V_{dc}}{2}\hat{i}_g\cos(\omega t)-\cancel{\frac{V_{dc}}{2}\Big[\frac{\hat{v}_g\hat{i}_g}{V_{dc}}\frac{1}{2}\cos(2\omega t)\Big]}\\ &\cancel{-\frac{1}{4}\hat{v}_g\hat{i}_g\cos(2\omega t)}+\frac{1}{4}\hat{v}_g\hat{i}_g-\\ &\frac{1}{4\frac{V_{dc}}{2}}\hat{v}_g^2\hat{i}_g\frac{1}{2}\Big[\cos(2\omega t+\omega t)+\cos(2\omega t-\omega t)\Big] \end{aligned} \tag{7}$$

This can be further developed to (8). Assuming modulation index of unity so that $\frac{V_{dc}}{2}=\hat{v}_g$:

$$=\frac{1}{4}\hat{i}_g\frac{V_{dc}}{2}\Big[1+\frac{3}{2}\cos(\omega t)-\frac{1}{2}\cos(3\omega t)\Big] \tag{8}$$

This proves that the injected circulating current mitigates the second harmonic component. It also lowers the fundamental oscillating component with 25 %. But on the downside it also introduces a component at the 3rd harmonic frequency, with a peak amplitude of 50 % in relation to the DC component. This is illustrated in Fig. 4 with waveform and FFT.

C. Filter Design

The last section showed that the filter needs to attenuate one large fundamental component, and a smaller 3rd harmonic component. A lowpass filter could be utilized to do this, but to attenuate such a low frequency as the fundamental component, very bulky components would be required. Therefore, a resonant filter is a more feasible choice. In Fig. 5 three different resonant filter arrangements are shown. All these filters can be tuned to attenuate a specific frequency. The double-tuned [11] can also attenuated two frequencies, which could be tuned to the fundamental and 3rd harmonic frequency. The C-type filter [12] provides a wider damping area which makes it easier to realize with real-world components. But in in this paper only the conventional single-tuned LC resonant filter will be investigated. This type of filter provides the best attenuation at the resonant frequency, which in this case is important regarding the large

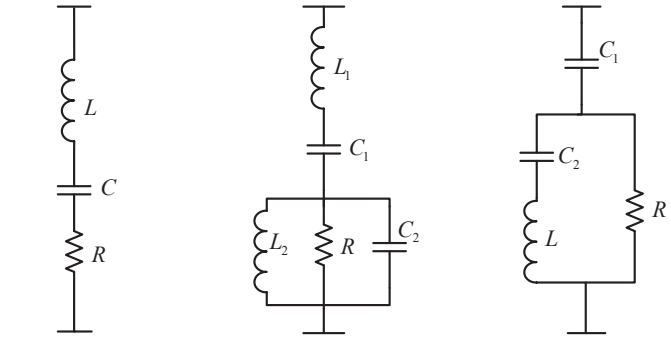

(a) Single-tuned (b) Double-tuned (c) C-type

Fig. 5. Different resonant filter arrangements

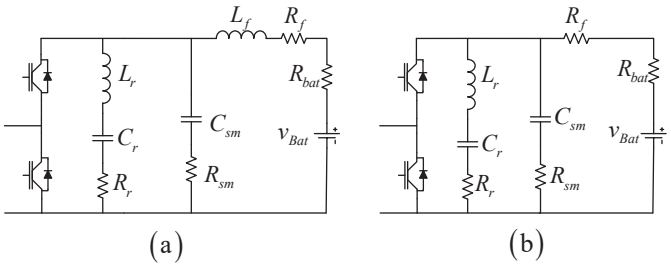

Fig. 6. Proposed filter

fundamental component it needs to filter.

The complete proposed filter is similar to the passive filter in [3], and is presented in Fig. 6. A resonant branch combined with a lowpass branch, (a) with lowpass inductor, and (b) without. The switches represents the submodule and the battery is modeled as a voltage source in series with the internal resistance.

First, to tune the resonant filter, the values of L_r and C_r where the resonant branch impedance is zero is located as,

$$j\omega L_r + \frac{1}{j\omega C_r} = 0 \tag{9}$$

Where, $j^2 = -1$ and $\omega = 2\pi f_r$, gives,

$$f_r = \frac{1}{2\pi\sqrt{L_r C_r}} \tag{10}$$

At this frequency the only impedance in the resonant branch is the resistance R_r. This frequency can be tuned to the fundamental frequency as.

$$L_r C_r = \left(\frac{1}{2\pi f_{fund}}\right)^2 \tag{11}$$

To further analyze this filter, the transfer function is obtained as,

$$TF(s) = \frac{I_{bat}}{I_{sm}} = \frac{Z_r \parallel Z_{sm}}{Z_r \parallel Z_{sm} + Z_{bat}} = \frac{n(s)}{d(s)} \tag{12}$$

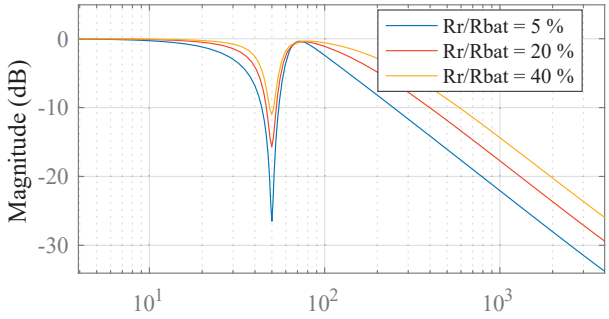

Fig. 7. Frequency response in Hz

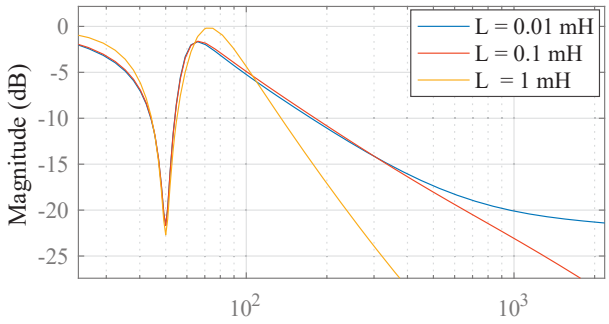

Fig. 8. Frequency response in Hz

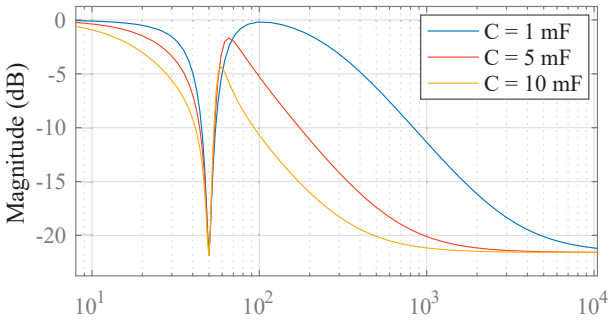

Fig. 9. Frequency response in Hz

Where $n(s)$ and $d(s)$ for the filter in Fig. 6(a) are given at the top of the next page. Setting $L_f = 0$ will give filter (b). The Bode plots of transfer function (12) is shown in Fig. 7, 8 and 9, where different filter component values are varied to analyze filter performance.

Fig. 7 show how battery internal resistance R_{bat} and resonant branch resistance R_r affects the frequency response. For each of the three lines, R_{bat} is decreased and R_r is increased. This shows that it is crucial for the performance of the resonant filter, that R_r is very small compared with R_{bat}. Since battery resistance typically is very low, especially for Li-ion and high capacity batteries, R_r should ideally be zero. Unfortunately there is always an ESR in real-world components, this should be minimized for optimal filter performance.

$$
\begin{aligned}
n(s) &= C_{sm}R_{sm}C_rL_rs^3 + \big[C_{sm}R_{sm}C_rR_r + C_rL_r\big]s^2 + \big[C_{sm}R_{sm} + C_rR_r\big]s + 1 \\
d(s) &= C_rC_{sm}L_fL_rs^4 + \big[C_rC_{sm}L_r(R_{bat}+R_f) + C_rC_{sm}L_fR_r + C_rC_{sm}R_{sm}(L_f+L_r)\big]s^3 + \\
&\quad \big[C_rC_{sm}R_r(R_{bat}+R_f) + C_rC_{sm}R_{sm}(R_{bat}+R_f) + C_rC_{sm}R_rR_{sm} + C_{sm}L_f + C_r(L_r+L_f)\big]s^2 + \\
&\quad \big[(C_r+C_{sm})(R_{bat}+R_f) + C_rR_r + C_{sm}R_{sm}\big]s + 1
\end{aligned}
$$

Fig. 8 show frequency response of filter (a), for differing inductance values on L_f. It shows that an inductance of roughly 1 mH is required before it will improve the damping of the 3rd harmonic component. At this size it also introduces a resonant top near the 2nd harmonic frequency. This could be problematic if the circulating current does not completely mitigate this component.

Also, this inductor needs to carry DC current. To avoid saturation, this could lead to a bulky component. Which finally leads to considering a case without this inductor.

Fig. 9 show how the capacity of the lowpass capacitor affects the frequency response of filter (b). And it shows that a high enough value will attenuate the 3rd harmonic even without the lowpass inductor.

D. Simple Loss Estimation

Both the injected circulating current and the interface filter will result in additional power loss for the system as a whole. Estimating these losses can be a comprehensive task, so the scope of this paper is limited to do a simplified estimation.

The injected circulating current will inevitably increase the arm currents that flow inside the converter. Increasing switching losses and conduction losses in the submodules, and in other ESRs inside the converter legs. The power losses in resistance are proportional to square of the arm currents RMS values, according to $P = RI^2$. Hence, increased RMS value of the arm current is calculated to estimate the additional internal converter losses.

With suppressed circulating current this gives.

$$
i_{arm}^{rms} = \sqrt{\frac{1}{T}\int_t^{t+T}\Big(\frac{\hat{i}_g}{2}\cos\omega t\Big)^2 dt} = \frac{1}{2\sqrt{2}}\hat{i}_g \tag{13}
$$

Then, injecting circulating current with peak amplitude of $\frac{\hat{v}_g\hat{i}_g}{2V_{dc}}$ which can be simplified to $\frac{\hat{i}_g}{4}$ with modulation ratio of 1 so that $\frac{V_{dc}}{2} = \hat{v}_g$, gives:

$$
i_{arm,inj}^{rms} = \sqrt{\frac{1}{T}\int_t^{t+T}\Big(\frac{\hat{i}_g}{2}\cos\omega t + \frac{\hat{i}_g}{4}\cos 2\omega t\Big)^2 dt} \tag{14}
$$

Doing the integration's in (14) results in:

$$
i_{arm,inj}^{rms} = \sqrt{\frac{1}{2}\Big(\frac{\hat{i}_g}{2}\Big)^2 + \frac{1}{2}\Big(\frac{\hat{i}_g}{4}\Big)^2} = \sqrt{\frac{5}{32}}\,\hat{i}_g \tag{15}
$$

This corresponds to an increase of $\frac{0.395}{0.354} = 11.6\,\%$, which will increase RI^2 losses with $24.5\,\%$. Considering the low internal losses in the MMC, this will result in less than 1% of total efficiency reduction.

The additional losses introduced in the filter will mainly be due to the ESRs in the resonant and lowpass branches. To estimate these power losses, lets assume that all the AC components, fundamental and 3rd harmonic, flow through them. This gives and RMS of

$$
\Big(i_{fnd} + i_{3rd}\Big)_{rms} = \frac{1}{\sqrt{2}}\Big(\frac{3}{2} + \frac{1}{2}\Big)\,i_{dc} = \sqrt{2}\,i_{dc} \tag{16}
$$

If all the AC components are to flow through the filter branches, that will imply that the ESRs must be very low. But instead lets consider a case where the ESRs are fairly high. $R_r = R_f = 0.5\Omega$ with $i_{dc} = 1A$ this gives

$$
P_{filter} = 0.5\Big(\sqrt{2}\Big)^2 = 1\,W \tag{17}
$$

To relate this loss to something, lets assume a battery voltage of 100 V, $V_{bat} = 100V$. This means that the battery power would be 100 W, and hence the filter loss would correspond to approximately 1 %.

III. Simulation and Lab

The proposed interface solution has been implemented in an MMC model built in Matlab/Simulink. Table I show the most important parameters. The AC side is loaded with pure ohmic resistances and power control is running open loop. A double-line-frequency negative dq-frame controller, [13], is implemented to inject the desired circulating current.

TABLE I
SIMULATION PARAMETERS

MMC parameters		Filter parameters	
Number of submodules per arm	$N_{sm} = 4$	L_f	10.13 mH
Arm inductance	$L_{arm} = 1$ mH	C_r	1 mF
Open circuit battery voltage	$V_{oc} = 300$ V	R_r	0.1 Ω
Load Resistance	100 Ω	C_{sm}	2 mF
Modulation index	$m = 1$	R_{sm}	0.01 Ω
Carrier frequency (PS PWM)	$f_{PWM} = 800$ Hz	L_f	0
Fundamental frequency	$f_{ac} = 50$ Hz	R_{bal}	2 Ω

Fig. 10 show the current that is flowing through the submodules before any filtering and only with suppressed

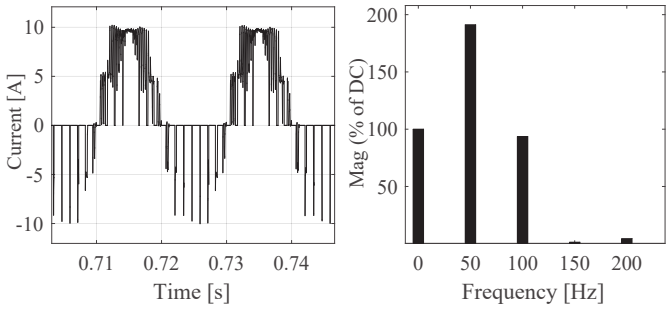

Fig. 10. Waveform and FFT of current flowing through submodule with suppressed circulating current

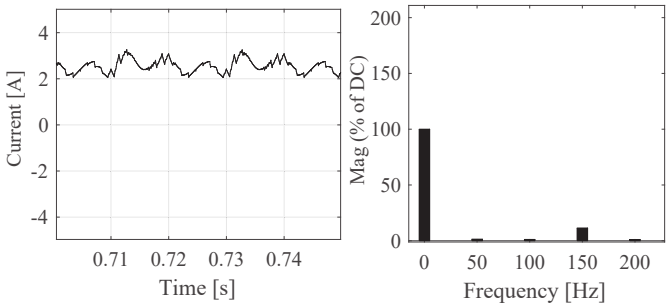

Fig. 11. Waveform and FFT of battery current with injected circulating current and passive interface filter

circulating current. Together with its FFT it shows very similar characteristics as was derived in section II. The 50 Hz component has a magnitude of 191 % and the 100 Hz 93.3 % relative to the DC component of 2.57 A.

Fig. 11 show the battery current with the given filter in place and with an injected circulating current corresponding to what was derived in (6). Together with its FFT it shows that the circulating current almost mitigates the 100 Hz component, now at 1.55 %. And the resonant filter mitigates the 50 Hz component down to 6.78 %. Also a 150 Hz component is now present with a magnitude of 12.8 %.

These simulations therefore back up the characteristics derived through section II.

A simple resonant filter of film capacitors and radially leaded inductors was soldered together in lab, Fig. 12, and run through a frequency sweep to reveal its resonant filter frequency response. With two paralleled capacitors on 100 μF as much as 50 mH inductance is needed to give a resonant frequency of 50 Hz. In lab the total ESR in the branch was 1.7Ω out of which 1.2Ω is due to the indcutors. For Li-ion and high capacity batteries this will result in poor filter performance. To significantly reduce the ESR, increasing capacitance and decreasing the inductance should be considered. Both measures resulting in lowered ESR. To realize such a filter in a feasible size, electrolytic capacitors needs to be used. Methods such as paralleling several capacitors and increasing

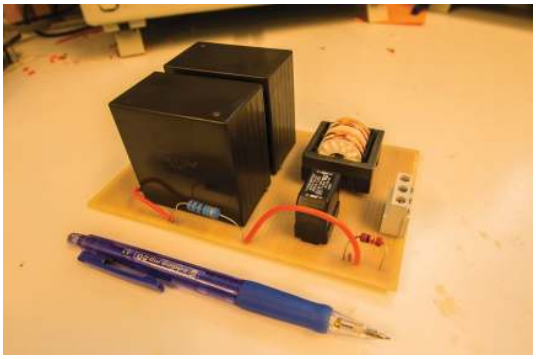

Fig. 12. Resonant filter in lab

cross section of the copper wire should also be employed to lower ESR further.

IV. Conclusion

This paper has investigated the two-legged solution of **1.** injecting a circulating current that cancels second harmonic arm power fluctuations and **2.** employing a passive filter between submodule and battery, to mitigate harmful AC currents that otherwise would flow through the battery in a split-battery MMC arrangement. Theoretical and simulation results indicates that this solution is capable of solving its intended task without reducing the efficiency of the converter significantly. Minimizing ESR in resonant branch of the filter is of high importance for the filter performance. Finally, providing a more reliable an less complex solution compared to the DC-DC converter interface which has been used in most literature.

References

[1] G. Wang *et al.*, "A review of power electronics for grid connection of utility-scale battery energy storage systems," *IEEE Transactions on Sustainable Energy*, vol. 7, no. 4, p. 17781790, Oct. 2016.

[2] M. Schroeder *et al.*, "Integration of batteries into a modular multilevel converter," *15th European Conference on Power Electronics and Applications*, pp. 1–12, 2013.

[3] M. Vasiladiotis, A. Rufer, and A. Bguin, "Modular converter architecture for medium voltage ultra fast ev charging stations: Global system considerations," in *Electric Vehicle Conference (IEVC)*, Greenville, USA, 2012.

[4] M. Vasiladiotis and A. Rufer, "Analysis and control of modular multilevel converters with integrated battery energy storage," *IEEE Transactions on Power Electronics*, vol. 30, no. 1, pp. 163–175, 2015.

[5] F. Gao *et al.*, "State-of-charge balancing control strategy of battery energy storage system based on modular multilevel converter," in *IEEE Energy Conversion Congress and Exposition (ECCE)*, Pittsburgh, USA, 2014.

[6] V. S. K. P. Prasanna, M. Sreedhar, "A comparative analysis of circulating current controllers for modular multilevel converters," in *Annual IEEE India Conference (INDICON)*, New Delhi, India, 2015.

[7] A. Korn, M. Winkelnkemper, and P. Steimer, "Low output frequency operation of the modular multi-level converter," in *IEEE Energy Conversion Congress and Exposition*, Atlanta, USA, 2010.

[8] ——, "A modular direct converter for transformerless rail interties," *IEEE International Symposium on Industrial Electronics*, pp. 562–567, July 2010.

[9] J. Kolb, F. Kammerer, and M. Braun, "Straight forward vector control of the modular multilevel converter for feeding three-phase machines over their complete frequency range," in *Annual Conference of the IEEE Industrials Electronics Society (IECON)*, Melbourne, Australia, 2011.

[10] M. Vasiladiotis *et al.*, "Accurate capacitor voltage ripple estimation and current control considerations for grid-connected modular multilevel converters," *IEEE Transactions on Power Electronics*, pp. 4568–4579, Sept. 2014.

[11] M. A. Zamani and M. Mohseni, "Damped-type double tuned filters design for hvdc systems," in *9th International Conference on Electrical Power Quality and Utilisation*, Barcelona, Spain, 2007.

[12] R. Dwyer, H. V. Nguyen, and S. G. Ashmore, "C filters for wide-bandwith harmonic attenuation with low losses," in *IEEE Power Engineering Society Winter Meeting, year = 2000, address = Singapore*.

[13] Q. Tu, Z. Xu, and L. Xu, "Reduced switching-frequency modulation and circulating current suppression for modular multilevel converters," *IEEE Transactions on Power Delivery*, vol. 26, no. 3, pp. 2009–2017, july 2011.